Pattern formation for NO+NH$_3$ on Pt(100) – 2D numerical results

Hannes Uecker

Mathematisches Institut I, D-76128 Universität Karlsruhe, hannes.uecker@math.uni-karlsruhe.de

Abstract

The Lombardo–Imbihl–Fink (LFI) model of the NO+NH$_3$ reaction on a Pt(100) surface consists of 7 coupled ODE. It shows stable relaxation oscillations with very sharp transitions. Here we study numerically the effect of linear diffusive coupling of these oscillators in 2D. We find different types of patterns, in particular phase clusters and standing waves, and a regime of standing wave turbulence. In models of related surface reactions such clustered solutions are known to exist only under a global coupling through the gas phase. This global coupling is replaced here by relatively fast diffusion of two variables which are kinetically slaved in the ODE.

1 Introduction

The deleterious effects of substances like NO in the atmosphere make it desirable to reduce these substances. The catalytic reduction of NO with NH$_3$ to the products N$_2$ and H$_2$O on a Pt(100) surface has been studied experimentally in [25]. This surface can switch between two substrate configurations, the catalytically active 1×1 phase with a bulk–like surface termination and a catalytically inert quasi–hexagonal reconstructed phase ("hex"). The stable state of the clean Pt(100) surface is the hex reconstruction but above a critical adsorbate coverage the 1×1 phase is more stable and the reconstruction is lifted. Thus an adsorbate-induced 1×1↔ hex phase transition is constituted. A realistic model for this reaction has been set up in [14]. It consists of 7 coupled ordinary differential equations (ODE) for $\theta_{NO}^{1\times1}, \theta_{NO}^{hex}, \theta_{1\times1}, \theta_{NH_3}^{1\times1}, \theta_{O}^{1\times1}, \theta_{N}^{1\times1}, \theta_{H}^{1\times1}$, which correspond to, in that order, the local coverages of NO on the 1×1–phase, of NO on the hex–phase, the fraction $\theta_{1\times1}$ of the surface in 1×1–phase, and to the local coverages of NH$_3$, O, N and H on the 1×1–phase. We write the ODE in abstract form as

$$\frac{\mathrm{d}}{\mathrm{d}t}X = f(X; p, T), \quad X \in \mathbb{R}^7, \quad f = (f_1, \ldots, f_7), \tag{1.1}$$

where $p \in \mathbb{R}^{11}$ is a vector of (fixed) temperature independent parameters. Moreover, (1.1) contains 11 rate constants depending by Arrhenius-law on temperature T, which we therefore display explicitly. In p there are two external (tunable) parameters, p$_{NO}$, and p$_{NH_3}$, acting as driving forces and corresponding to a constant supply of NO and NH$_3$, respectively, from the gas phase.

The model shows oscillations in a temperature range from 404K to 433K, similar to the experiment. However, the oscillations in the model are strongly anharmonic while in the experiment they appear to be much more harmonic. In section 2.1 we plot typical periodic

orbits of (1.1), but we will not repeat in detail the properties of this ODE; see App.A for the equations, and [14, 24] for discussion and numerical analysis of (1.1). Here we continue work [23] on the effect of linear diffusive coupling of these ODE oscillators and consider the 2D case

$$\frac{\mathrm{d}}{\mathrm{d}t}X(t,x) = f(X(t,\vec{x}); p, T) + M(T)\Delta X(t,\vec{x}), \qquad (1.2)$$

where $M(T)$ is the diagonal diffusion matrix depending on T. The patterns obtained in 1D in [23] were classified into 4 groups (see sec.2.4 for illustration): bulk oscillations (BO) aka synchronization, standing waves (SW), phase clusters (PC), and phase waves (PW). Even in 1D a systematic study of the dependence of the patterns on the various parameters and the initial conditions is hard. In 2D, additional geometric effects play an important role and for SW and PC lead to very long transients, and to a turbulent SW regime. Hence, here we essentially restrict to presenting examples of these patterns.

Bulk oscillations (synchronization) means that the whole surface oscillates homogeneously in the limit cycle of (1.1), while in both SW and PC the oscillations are organized into macroscopic areas (clusters) in such a way that the phase changes from one area to the next in a regular way, with phase shifts of half a period. The difference between SW and PC is that in SW the phase–pattern has an intrinsic spatial wave–length, while in PC the clusters have no intrinsic size and grow until the whole domain is split into only 2 clusters. Here we follow [1, 18, 8, 3] in the terminology, but also loosely term both SW and PC as clustering. This clustering requires substantial deviations from the periodic ODE orbits at the cluster boundaries. Phase waves (PW) means that the phase changes smoothly and each individual oscillator is always close to the periodic ODE orbit.

One effect of the clustering is that it reduces the periods of oscillations of macroscopic (i.e. spatially averaged) quantities by a factor of (roughly) 2. Moreover, while (1.1) has relaxation oscillations with very sharp transitions, the averaged quantities oscillate more harmonically. Both effects together yield a much better agreement of the model with experimental data [14, fig.7].

The transitions between the different regimes are rather delicate. The system is most sensitive with respect to the (relatively small) NO diffusions on the $1{\times}1$ and the hex phase, respectively. This agrees well with the analysis in [24] where it is shown that $\theta_{NO}^{1\times1}, \theta_{NO}^{hex}$ and $\theta_{1\times1}$ are the "master" dynamic variables for (1.1) (in the oscillatory regime) while the remaining four are "slaved". However, $\theta_{1\times1}$ does not diffuse, which gives NO–diffusion its special importance.

Of course, synchronization, PC, SW and PW (and the competition between these patterns) are also very interesting from a theoretical point of view. Phase waves for oscillators close to a Hopf point can be analyzed using phase diffusion equations; see, e.g., [12, 15, 26]. However, relaxation oscillators may behave quite differently under (weak) coupling than harmonic oscillators [21, 9, 16]; in particular, under certain assumptions phase waves cease

to exist; see [23] for discussion and further references. On the other hand, SW can be generated in simple reaction–diffusion systems via the so called wave–bifurcation [28, 11]. However, this again corresponds to a (roughly) harmonic time (and space) dependence.

In surface catalysis, clustering has been intensively studied for the CO oxidation on Pt(110), both experimentally and theoretically [1, 7, 8, 19, 18, 3, 5, 4]. Here the reaction–diffusion models have considerably simpler ODE dynamics than (1.1) (3 dimensional or, in a refined version, 4 dimensional), but additional to the surface diffusion there is a *global* coupling through the gas phase in the spatially extended system. Moreover, external forcing [18] and/or global delayed feedback [10, 3, 5, 4] have been used to *control* the pattern formation in this system; see also [27] for clustering in a reaction–diffusion model of the Belousov–Zhabotinsky with 2 dimensional kinetics and a global feedback.

The ODE (1.1) can also be reduced to a 3 dimensional system

$$\frac{\mathrm{d}}{\mathrm{d}t}y = g(y; p, T), \quad y = \begin{pmatrix} \theta_{\mathrm{NO}}^{1\times 1} \\ \theta_{\mathrm{NO}}^{\mathrm{hex}} \\ \theta_{1\times 1} \end{pmatrix}, \quad g(y) = \begin{pmatrix} f_1(\theta_{\mathrm{NO}}^{1\times 1}, \theta_{\mathrm{NO}}^{\mathrm{hex}}, \theta_{1\times 1}, h(y)) \\ f_2(\theta_{\mathrm{NO}}^{1\times 1}, \theta_{\mathrm{NO}}^{\mathrm{hex}}, \theta_{1\times 1}, h(y)) \\ f_3(\theta_{\mathrm{NO}}^{1\times 1}, \theta_{\mathrm{NO}}^{\mathrm{hex}}, \theta_{1\times 1}, h(y)) \end{pmatrix}, \quad (1.3)$$

for the slow variables y by elimination of the fast variables $z = (\theta_{\mathrm{NH}_3}^{1\times 1}, \theta_{\mathrm{O}}^{1\times 1}, \theta_{\mathrm{N}}^{1\times 1}, \theta_{\mathrm{H}}^{1\times 1})$ [24]. Chemically, the key role of NO is due to the fact that in (1.1) the lifting of the hex recon-struction proceeds through NO adsorption. The reduction of dimension in (1.3) is of course advantageous both analytically and numerically. Naively, we may then study the reaction diffusion problem

$$\frac{\mathrm{d}}{\mathrm{d}t}y = g(y; p, T) + M_{\mathrm{red}}\Delta y, \quad M_{\mathrm{red}} = \mathrm{diag}(D_{\mathrm{NO}}^{1\times 1}, D_{\mathrm{NO}}^{\mathrm{hex}}, 0). \quad (1.4)$$

However, as already discussed in [23], although the error between (1.1) and (1.3) is very small, obviously all the influence of the (relatively fast) diffusion of NH_3 and H is lost in going from (1.2) to (1.4). On the other hand, the elimination of kinetically slaved variables from PDE like (1.2) can be done analytically only in special cases, see, for instance [17], and numerically yields little advantage.

Note that (1.4) corresponds to (1.2) in the limit $D_{\mathrm{NH}_3}, D_{\mathrm{H}} = 0$. We find that no clustering occurs in this limit or even for relatively slow diffusion of NH_3 and H. This shows that, additional to the relaxation type of the oscillations, a key ingredient for clustering in (1.2) is a *nonlocal* (or long range) coupling due to relatively fast diffusion of the kinetically slaved variables $\theta_{\mathrm{NH}_3}^{1\times 1}$ and $\theta_{\mathrm{H}}^{1\times 1}$.

The most important difference between the 1D simulations in [23] and the 2D simula-tions presented here are curvature effects. The net result is that in 2D, curved SW (which may look similar to target patterns) are unstable and slowly relax to quasi–1D SW in a very long transient process. Moreover, while in the parameter regimes considered in [23] all solutions are quite regular and eventually become periodic in 1D, in 2D for the same

parameters we find very irregular SW on large domains, i.e., we find a turbulent standing wave regime.

The preparatory sec.2 contains remarks on the periodic orbits for (1.1), the diffusion constants, the numerical method, and the choice of initial conditions for (1.2). In sec.3 we present our results. Conclusions are summarized in sec.4, while App.A contains the ODE (1.1). Some movies of the solutions are available via internet [22].

2 The setup

2.1 The periodic ODE–orbits

Figure 1, taken from [23], shows periodic orbits $\gamma(T)$ for (1.1) at $T = 410, 420, 430$K. In (a) we present all 7 dynamic variables, while (b) shows the chemically interesting production rates $r_{N_2} = 0.5 N_s k_9 (\theta_N^{1\times1})^2 / \theta_{1\times1}$ of N_2 and $r_{H_2O} = N_s k_8 \theta_O^{1\times1} \theta_H^{1\times1} / \theta_{1\times1}$ of H_2O, where $N_s = 1.3 \times 10^{15}$ cm^{-2} is the concentration of surface sites. The most important conclusions
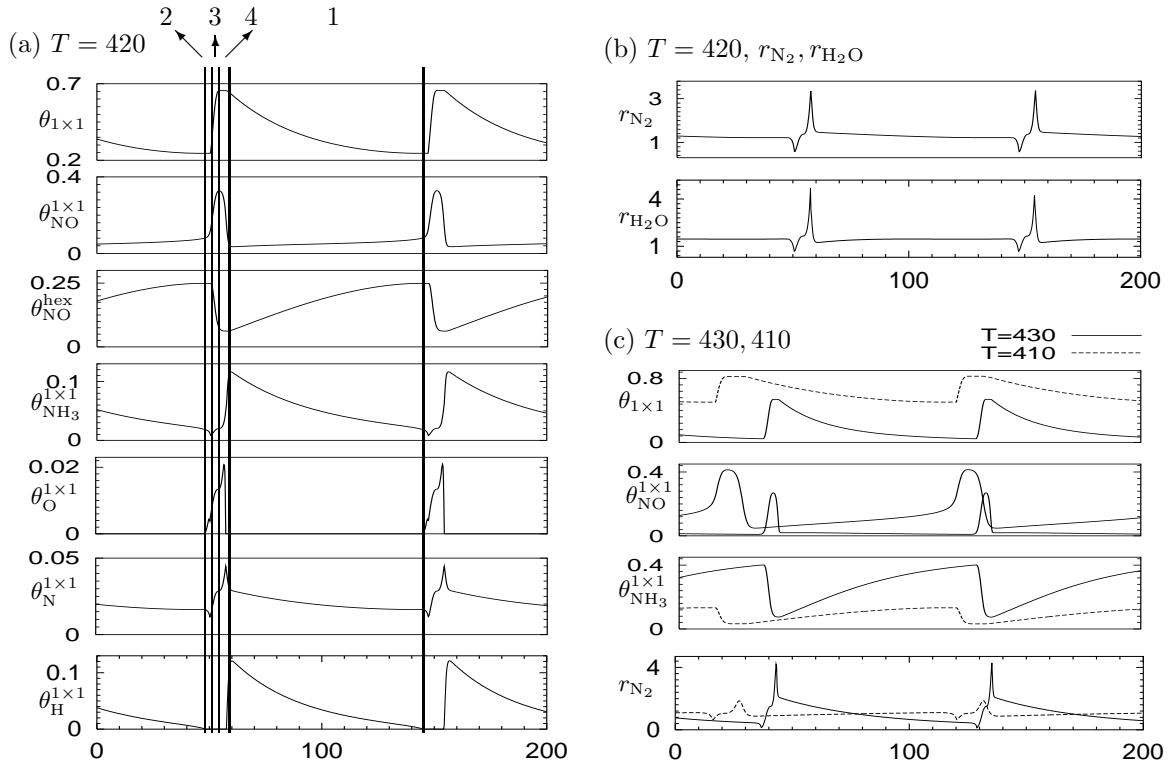

Figure 1: (a) periodic ODE–orbits at $T = 420$K, (b) production rates at $T = 420$K, (c) $\theta_{NO}^{1\times1}, \theta_{NO}^{hex}, \theta_{1\times1}, r_{N_2}$ at $T = 410, 430$K; time in s, coverages are dimensionless, production rates r_{N_2}, r_{H_2O} in 10^{14}cm^{-2}s^{-1}. Quantities from these ODE orbits will henceforth be refered as, e.g., $\theta_{1\times1}^{ODE}$.

from [14, 24] are as follows. One period is divided into four segments. We plot $\theta_{1\times1}$ first

process	parameter	$\tilde{E}$ (kJ mol^{-1})	value at 420K (cm^2 s^{-1})
NO–diffusion (1×1)	$D_1 = D_{\text{NO}}^{1\times1}$	28	3.3×10^{-7}
NO–diffusion (hex)	$D_2 = D_{\text{NO}}^{\text{hex}}$	24	1×10^{-6}
N.A.	$D_3 = 0$	N.A	always=0
NH$_3$–diffusion	$D_4 = D_{\text{NH}_3}$	15	1.4×10^{-5}
O–diffusion	$D_5 = D_{\text{O}}$	N.A.	always set to 0
N–diffusion	$D_6 = D_{\text{N}}$	N.A.	always set to 0
H–diffusion	$D_7 = D_{\text{H}}$	18	5.7×10^{-7}

N.A. means not applicable

Table 1: Diffusion energies and constants. For convenience we write $\vec{E} = (\tilde{E}_{\text{NO}}^{1\times1}, \tilde{E}_{\text{NO}}^{\text{hex}}, \tilde{E}_{\text{NH}_3}, \tilde{E}_{\text{H}})$.

since the decay of $\theta_{1\times1}$ in segment 1 sets the slowest time scale in the largest segment; here all other variables follow $\theta_{1\times1}$ adiabatically. This breaks down in segment 2, where adsorbtion of NO starts the hex→1×1 phase transformation in segment 3. In segment 4 the so called "surface explosion" occurs with a rapid production of N$_2$ and H$_2$O. The NH$_{\text{x,ad}}$/H$_{\text{ad}}$ layer built up this way is unable to stabilize the 1×1 phase, and the process repeats with the slow relaxation to the hex phase in segment 1.

The temperature dependence is illustrated in (c). For lower T the (average) fraction $\theta_{1\times1}$ of the 1×1 phase increases, while the amplitude of the oscillations and the reaction rates decrease, and vice versa for higher T. The period t_0 also depends on T but only slightly in the middle of the oscillatory regime considered here. We have $t_0(420) \approx 97$s. Below the lower threshold ($T \approx 404K$) for oscillations the surface is completely in the 1×1 phase ($\theta_{1\times1} = 1$), while above the upper threshold ($T \approx 433K$) it is in the hex phase ($\theta_{1\times1} = 0$). In both cases, the production rates r_{N_2} and $r_{\text{H}_2\text{O}}$ are zero. For the reaction diffusion problem (1.2) two observations from fig.1 are most important: the smaller (larger) amplitudes at lower (higher) temperatures yield smaller (larger) spatial gradients for oscillators with shifted phases, and the transitions become less (more) sharp for lower (higher) T; see [23] and sec.4.

2.2 The diffusion constants

In choosing the diffusion constants for Pt(100)/H,N,O,NO,NH$_3$ we follow the arguments given in [23], based on [20, 2]. In the temperature range considered here, O and N can be considered immobile. As usual, we approximate the remaining D_i using the Arrhenius–law $D_i = \nu e^{-\tilde{E}_i/RT}$, where $R = 8.3144$ J K^{-1}mol is the universal gas constant, $\nu = 0.001$ cm^{2}s^{-1} is a common prefactor, and $\tilde{E}_i$ is the activation energy for diffusion of the respective species. This yields the data in table 1. However, these data should be seen as rough estimates only, hence as a starting point for the numerical simulations.

The diffusion constants differ quite significantly in size. We call diffusion of $NO_{1\times 1}$ and NO_{hex} relatively slow and that of H and NH_3 relatively fast. In this sense (strictly speaking for $D_{\text{NO}}^{1\times 1} = D_{\text{NO}}^{\text{hex}} = 0$) (1.2) is related to the model problem in [13] where a field of oscillators is coupled by diffusion through a passive medium. In sec.3 we find that the "typical pattern size" l_p for (1.2) at $T{=}420$ is of the order of 0.01cm. Hence $\sqrt{D_{\text{NH}_3}\tau}{\approx}2.4{\times}10^{-3}$cm and $\sqrt{D_{\text{H}}\tau} \approx 1.8{\times}10^{-3}$cm, where $\tau = 1$s is our time–scale, are roughly of the magnitude as l_p and diffusions of $\theta_{\text{NO}}^{\text{hex}}$ and $\theta_{\text{N}}^{1\times 1}$ introduce a nonlocal but also nonglobal coupling, where local (global) coupling would correspond to $\sqrt{D_{\text{NH}_3}\tau} \ll l_p$ ($\sqrt{D_{\text{NH}_3}\tau} \gg l_p$).

Henceforth, T, $\tilde{E}_i$ and D_i will be given without units; it is understood that T is in Kelvin and that the diffusion energies are in $\text{kJ}\,\text{mol}^{-1}$ and the diffusion constants in $\text{cm}^2\,\text{s}^{-1}$.

2.3 Numerical method and system size

To discretize (1.2) we choose a system size L (in cm), and consider $n \times n$ oscillators $X(\cdot, i, j) = X(\cdot, x_i, y_j)$ at $(x_i, y_j) = (i\delta, j\delta)$, $i, j = 1, \ldots, n$, $\delta = L/(n-1)$, with periodic boundary conditions. The numerical scheme is the same as in [23]: a split–step method, where the ODE–part is integrated using the linearly implicit solver `limex` [6, section 6.4] (available online at `www.zib.de/SciSoft/CodeLib/ivpode.en.html`) and the linear PDE–part $\frac{d}{dt}X = M\Delta X$ using an implicit Fourier spectral method. In our simulations we use $\delta = 0.0005$cm and the average effective time steps are about $dt = 0.001 \sim 0.01$ s (depending on the parameters).

The experimental data in [25] was reported for a sampled area of about 1mm^2. Here we consider smaller samples ($n = 64$, $\delta = 0.0005$ cm, and hence $L{=}0.032$ cm in all simulations except the last). Using 64×64 gives sufficiently many oscillators to show the mechanism.

The initial conditions (IC) for (1.2) were chosen as localized perturbations of the point $Z_0 = (0.03, 0.24, 0.22, 0.5{\times}10^{-6}, 0.01, 0.02)$ which is roughly near the end of segment 1 of the periodic orbit $\gamma(420)$, cf. fig.1. That means, we first assign $X|_{t=0}(i, j) = Z_0$ to all oscillators, then choose $l \in \{0, \ldots, 7\}$ and $a \in \mathbb{R}$, and add a perturbation of amplitude a to the lth component in part of the domain. In formulas, we set

$$X_l|_{t=0}(i,j) = \begin{cases} z_l + a, & (i,j) \in \mathcal{I}, \\ z_l & \text{elsewhere}, \end{cases} \tag{2.1}$$

where $\mathcal{I} \subset \mathbb{N}^2$ is an index set. For some $k < n$ we set $\mathcal{I} = \mathcal{I}_k = \{(i,j) : 0 \leq i, j \leq k\}$, i.e., we perturb in a square in the upper left. Some random initial conditions were also used.

The synchronized solution X_{BO} is asymptotically stable in the parameter regime given by table 1. Hence, in (2.1) we need sufficiently large k and/or a, depending on l, to push the system at least transiently away from X_{BO}. As should be expected from the ODE reduction (1.3), the easiest way to perturb the system away from X_{BO} is to introduce perturbations in $\theta_{\text{NO}}^{1\times 1}, \theta_{\text{NO}}^{\text{hex}}$ or $\theta_{1\times 1}$, i.e., to choose $l \in \{1, 2, 3\}$. For the sake of brevity we restrict to

6

perturbations in $\theta_{1\times 1}$ ($l = 3$), fix $k = n/4$, and vary a. Note that this way we add a perturbation to a non diffusive component and hence the system can only be driven back to or further away from X_{BO} by coupling to the diffusive components.

We focus on plotting $\theta_{1\times 1}(t, x, y)$ as the main diagnostic for (1.2). As explained in sec.2.1, $\theta_{1\times 1}$ sets the timescale in the largest segment 1 of the ODE–orbits. Hence, for the reaction–diffusion problem we expect that for given $\theta_{1\times 1}$ the remaining variables can roughly be read from fig.1, at least at values in segment 1 of the ODE–orbit. This turns out to true [23]. To visualize the spatio–temporal patterns we a use 2d–plots of $\theta_{1\times 1}$ at fixed time, and space–time plots of $\theta_{1\times 1}$ along lines through the 2d domain. These plots are further complemented with diagnostics like local time series and the spatial average $\langle\theta_{1\times 1}\rangle(t) = \frac{1}{n^2}\sum_{i,j=1}^{n}\theta_{1\times 1}(t, i, j)$.

2.4 Classification in 1D

In figure 2 we show greyscale plots from [23] illustrating synchronization, PC, SW and PW, in 1D, where the initial conditions are the 1D–analog of (2.1). All the solutions become periodic after a rather short time transient.
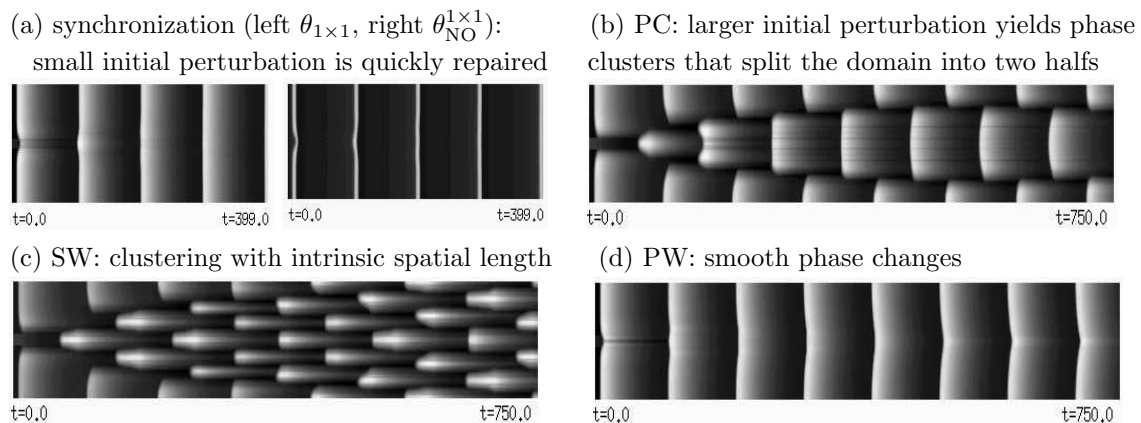
(a) synchronization (left $\theta_{1\times 1}$, right $\theta_{\mathrm{NO}}^{1\times 1}$): small initial perturbation is quickly repaired

(b) PC: larger initial perturbation yields phase clusters that split the domain into two halfs

(c) SW: clustering with intrinsic spatial length

(d) PW: smooth phase changes

Figure 2: Examples from [23] for synchronization, PC, SW and PW in 1D; $T = 420$, greyscale plots of $\theta_{1\times 1}(t, x)$ (and $\theta_{\mathrm{NO}}^{1\times 1}(t, x)$ in (a)); horizontal axis t, vertical axis x, spatial size $L = 0.0395$cm. The parameters are $\vec{E} = (28, 24, 15, 18)$ in (a),(b); $\vec{E} = (30, 22, 15, 18)$ in (c), $\vec{E} = (28, 22, 25, 25)$ in (d).

3 Simulations

We restrict to presenting examples of different patterns at $T = 420$. Temperature dependence is discussed below. The synchronized solution is asymptotically stable near the parameter regime given in table 1. Hence we directly start with a more interesting solution.

3.1 Phase clusters

In our first simulation we use the diffusion data from table 1, $n = 64$, and initial conditions according to (2.1) with $k = 16$ and $a = 0.1$. This yields the 2D analog of PC as we checked
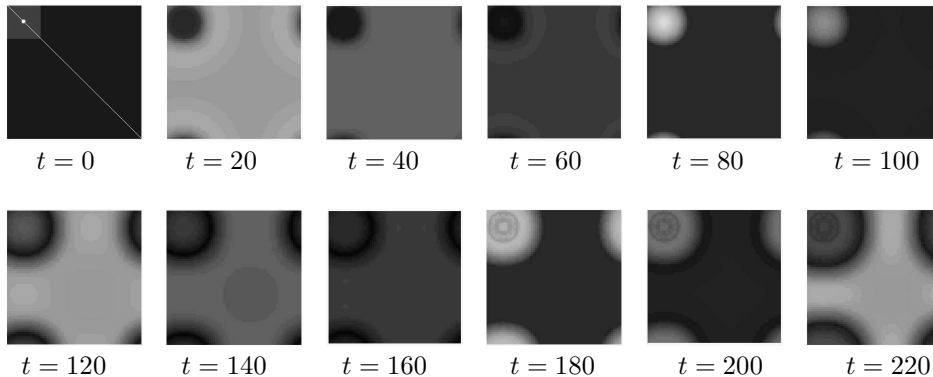

| $t = 0$ | $t = 20$ | $t = 40$ | $t = 60$ | $t = 80$ | $t = 100$ |

| $t = 120$ | $t = 140$ | $t = 160$ | $t = 180$ | $t = 200$ | $t = 220$ |

Figure 3: $\delta = 0.0005cm$, $n = 64$, $\vec{E} = (28, 24, 15, 18)$, greyscale snapshots of $\theta_{1\times1}$ $z_{\text{scal}} = 0.2, 0.9$. The small initial perturbation evolves into two phase clusters with phase shift of half a period. The white dot and the diagonal line at $t = 0$ mark the position $\vec{x}_1$ for the local time series and the diagonal for the space-time plots in fig.4.

by running the simulation on a larger domain. Figure 3 shows snapshots of $\theta_{1\times1}(t, \cdot)$. The greyscales are linear interpolations between z_{min}=black=0.2 and z_{max}=white=0.8; in the following this is denoted by $z_{\text{scal}} = z_{\text{min}}, z_{\text{max}}$. Near $t = 0$, the larger value of $\theta_{1\times1}$ in the top left corner inhibits the NO adsorption; this then inhibits the $1\times1\leftrightarrow$ hex phase transition in this part of the surface until $\theta_{1\times1}$ has sufficiently decayed at $t \approx 62$. For larger t we thus obtain a PC solution: one circular cluster roughly fills the top left quarter of the domain and the other fills the rest of the domain. In fig.4(a),(b) we show space-time plots of the solution in fig.3 along the left boundary (vertical line data) and the diagonal. Both clearly show the evolution towards the PC solution. During this process the cluster size slowly adjusts. Unlike the 1d case there is no phase balancing: the cluster in the top left quarter stays smaller in area than the other one. This is probably due to curvature since one cluster is convex while the other is concave. For $t > 1400$ and up to simulation time $t = 4000$ this solution stays nearly perfectly time periodic. However, in light of sec.3.3 this may still be a transient regime with an extremely long transient, see below. The time series in fig.4(c) illustrates that the solution at the marked point is close to (but not identical) to the limit cycle $\gamma(420)$ of the ODE. More detailed inspection of the solution shows that this is not true for oscillators at the cluster boundaries, as should be expected. The average $\langle\theta_{1\times1}\rangle$ is a very simple diagnostic for clustering (as opposed to phase waves, see sec.3.2): it has two maxima during one ODE period. Finally we show diagonal space time plots of two other components of the solution from fig.3 (a,b), and also 3D plots of the solution at $t = 730$ and $t = 775$ (c–e). Figure 5 (a),(b) show that $\theta_{\text{NO}}^{1\times1}, \theta_{\text{H}}^{1\times1}$ do indeed follow $\theta_{1\times1}$ according to the

(a) space–time plot of $\theta_{1\times1}$ at the left boundary

(c) time–series, $\langle\theta_{1\times1}\rangle$, $\theta_{1\times1}(\vec{x}_1)$ (dashed), $\theta_{1\times1}^{\mathrm{ODE}}$ (points)

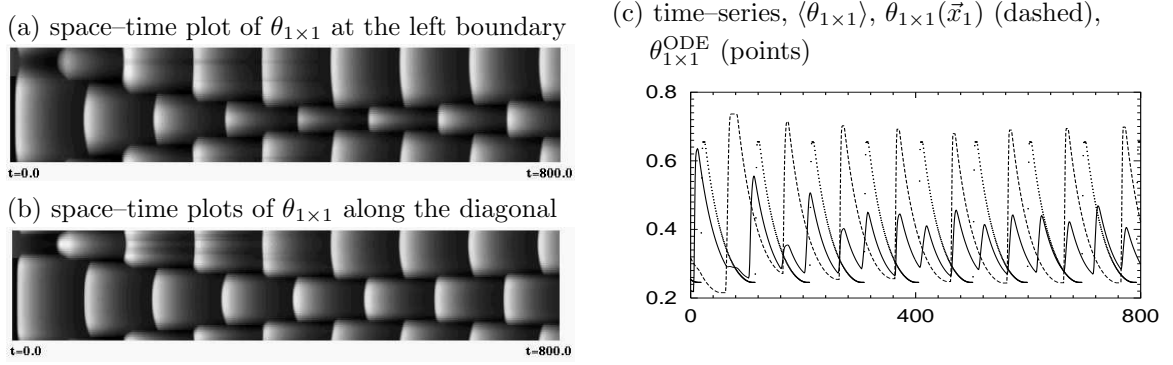(b) space–time plots of $\theta_{1\times1}$ along the diagonal

Figure 4: Diagnostics for fig.3, $z_{\mathrm{scal}} = 0.2, 0.9$; $\vec{x}_1$ is the point marked in fig.3.

ODE orbit, except at the cluster boundaries. This also holds for the remaining components (not shown). Moreover, (b) (and also (d)) illustrates that $\theta_{\mathrm{N}}^{1\times1}$ is more smooth than the non–diffusive component $\theta_{1\times1}$ or the component $\theta_{\mathrm{NO}}^{1\times1}$ with its slow diffusion. The plots (c–e) correspond to a time–difference of about half an ODE period and further illustrate the clustering seen in fig.4 and (a,b) near $t = 800$.
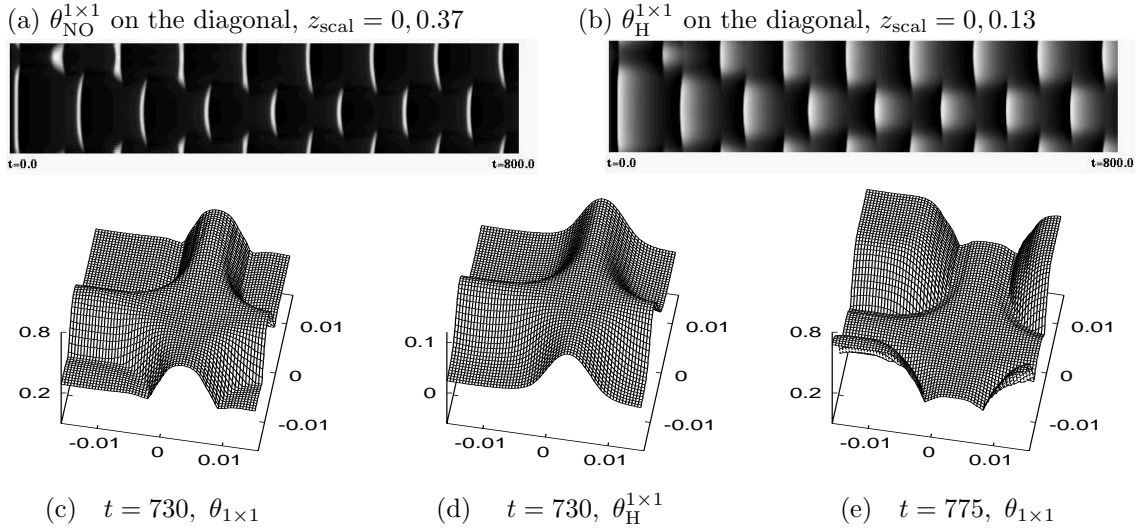
(a) $\theta_{\mathrm{NO}}^{1\times1}$ on the diagonal, $z_{\mathrm{scal}} = 0, 0.37$

(b) $\theta_{\mathrm{H}}^{1\times1}$ on the diagonal, $z_{\mathrm{scal}} = 0, 0.13$

(c) $t = 730$, $\theta_{1\times1}$

(d) $t = 730$, $\theta_{\mathrm{H}}^{1\times1}$

(e) $t = 775$, $\theta_{1\times1}$

Figure 5: Diagonal space time plots (a,b) illustrating that $\theta_{\mathrm{NO}}^{1\times1}, \theta_{\mathrm{H}}^{1\times1}$ follow $\theta_{1\times1}$ according to the ODE orbit except at the cluster boundaries. 3D plots (c–e), illustrating the clustering near $t = 800$ and the higher smoothness of $\theta_{\mathrm{H}}^{1\times1}$ compared to $\theta_{1\times1}$.

3.2 Phase waves

Figure 6 gives an example of a phase wave (PW). We use the same IC as in fig.3 but now $\vec{E} = (28, 24, 30, 30)$. Hence diffusion of $\theta_{\mathrm{NH}_3}^{1\times1}$ and $\theta_{\mathrm{N}}^{1\times1}$ is now slower than that of $\theta_{\mathrm{NO}}^{1\times1}$ and $\theta_{\mathrm{NO}}^{\mathrm{hex}}$. Consider the bottom line of fig.6: $\theta_{1\times1}(\vec{x}_1)$ has started to grow at $t \approx 190$, where $\vec{x}_1$

9

is the same point as in fig.3. This triggers a circular front which sweeps the domain. At $t \approx 202$ this front collides with itself due to the periodic boundary conditions. We conclude
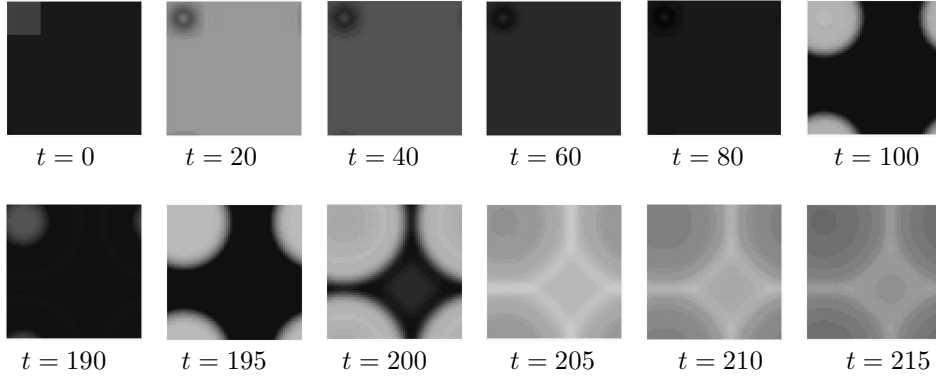

Figure 6: $n = 64$, M=(28,24,30,30), greyscale snapshots of $\theta_{1\times1}$, $z_{\text{scal}} = 0.2, 0.9$. The bottom line shows the sweeping of a phase wave through the domain.

that it is the nonlocal coupling by fast diffusion of $\theta_{\text{NH}_3}^{1\times1}, \theta_{\text{N}}^{1\times1}$ that prevents, for instance, the solution at $t = 80$ in fig.3 to trigger a similar front. Hence this fast diffusion is a key ingredient for the clustering.

Figure 7 presents the diagnostics for fig.6. For $t > 450$ the profiles in the line data roughly keep their shape and the solution is essentially periodic. The time–series shows that $\langle\theta_{1\times1}\rangle$ is slightly smeared out by the PW compared to the sharp transitions in $\theta_{1\times1}^{\text{ODE}}$. On larger domains we can also produce longer fronts which further smear out the transitions

Figure 7: Diagnostics for fig.6; $\vec{x}_1$ is the same point as marked in fig.3. From left: vertical line data, diagonal line data ($z_{\text{scal}} = 0.2, 0.9$), time–series, $\langle\theta_{1\times1}\rangle(t)$, $\theta_{1\times1}(t, \vec{x}_1)$ (dashed), $\theta_{1\times1}^{\text{ODE}}(t)$ (points).

in $\langle\theta_{1\times1}\rangle$ (see [23] for 1d examples). In PW, every oscillator is always quite close to $\gamma(420)$, with some small deviations only during the collisions of the fronts (e.g., $t = 205, 210$ in fig.6). Hence, in contrast to clustered solutions this situation should be describable by pure phase models [12, section 4]. Here we are more interested in clustered solutions, and now turn to SW.

3.3 Standing waves

In [23] it was found that in 1D (in the clustering regime, i.e., for large D_{NH_3}, D_{H}) the diffusions of $\theta_{\text{NO}}^{1\times1}$ and $\theta_{\text{NO}}^{\text{hex}}$ play the following roles: decreasing (increasing) $D_{\text{NO}}^{1\times1}$ ($\tilde{E}_{\text{NO}}^{1\times1}$)

may switch the system from PC (clustering with no intrinsic length scale) to SW (clustering with intrinsic length scale) and for SW decreases the spatial size of the clusters. Decreasing (increasing) D_{NO}^{hex} ($\tilde{E}_{NO}^{hex}$) acts the other way round. See also fig.2(b,c) for illustration in 1D. We now illustrate the similar effect in 2D.

In fig.8 we set $\vec{E} = (30, 22, 15, 18)$ and use the same initial conditions as in fig.3. The initial evolution looks roughly the same as in fig.3. However, at $t = 160$ we see that now
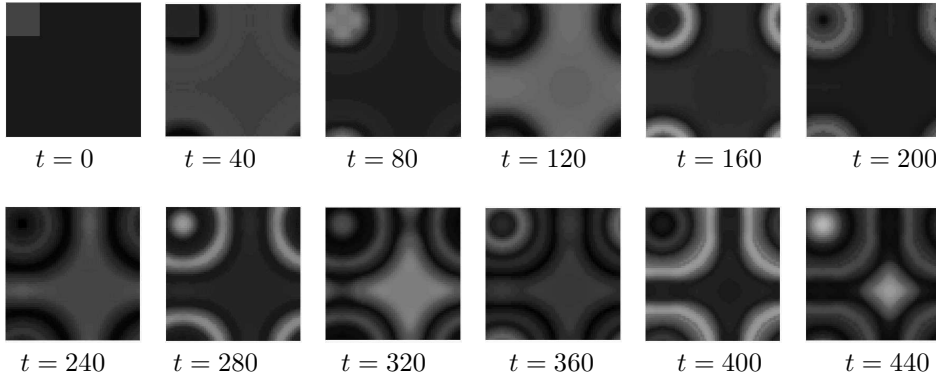

Figure 8: $n = 64, \vec{E} = (30, 22, 15, 18)$, greyscale snapshots of $\theta_{1\times1}$, $z_{\text{scal}} = 0.2, 1$. The initial evolution yields the SW analog to fig.2(c) in 2D, i.e., a solution with small clusters with intrinsic width of about 0.005cm. However, this is a transient behavior, see fig.10.

the top left corner itself starts to split into annular clusters, similar to a target pattern. Likewise, in the remaining part of the domain a banded structure appears where the bands of equal phase have a width of approximately 0.005cm. Hence we conclude that the clusters now have an intrinsic spatial scale. Therefore this solution is called a standing wave. This evolution can also be clearly seen in the space–time plots of fig.9. The average $\langle\theta_{1\times1}\rangle$ again oscillates with approximately half the ODE period. Moreover, the small clusters are associated with substantial deviations of individual oscillators from the ODE orbit also in the center of clusters; see, e.g., $\theta_{1\times1}(\vec{x}_1)$ around $t = 200$ to 280, which has about twice the amplitude of $\theta_{1\times1}^{\text{ODE}}$. The annular SW centered in the top left quadrant determines the
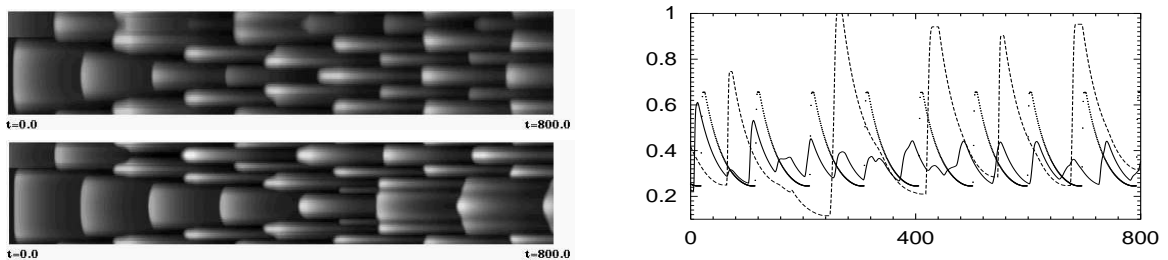

Figure 9: Diagnostics for fig.8; vertical (top left) and diagonal (bottom left) line data ($z_{\text{scal}} = 0.2, 1$), $\langle\theta_{1\times1}\rangle$, $\theta_{1\times1}(\vec{x}_1)$ (dashed), $\theta_{1\times1}^{\text{ODE}}$ (points), where $\vec{x}_1$ is the same point as marked in fig.3.

dynamics up to $t \approx 1000$. However, it is not stable. Therefore, triggered by unavoidable

numerical errors the solution looses its symmetry across the diagonal for $t > 1000$. A second transient regime sets in, where the clusters appear in interesting shifting patterns that become gradually more irregular. However, near $t \approx 2400$ a new structure appears which consists of horizontal bands of equal phase. This is clearly visible at $t = 3000$ in fig.10. For $t > 3000$ these bands slowly smooth out and adjust their spacing, and for $t > 4000$ we have a quasi 1–dimensional SW.

| $t = 1000$ | $t = 1200$ | $t = 1400$ | $t = 1600$ | $t = 1800$ | $t = 2000$ |

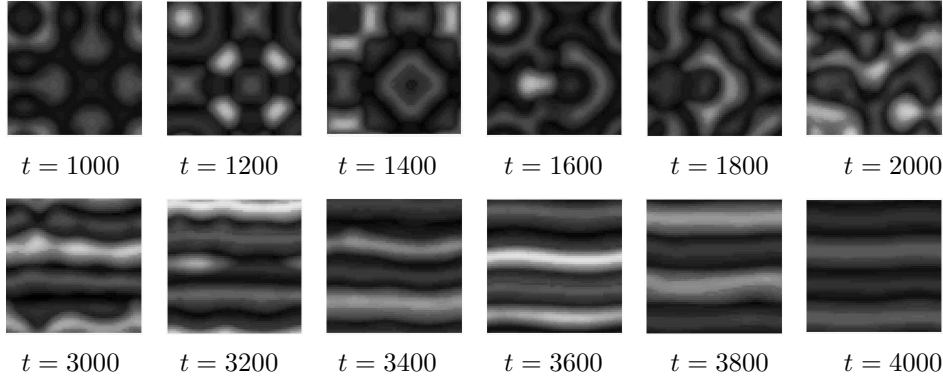| $t = 3000$ | $t = 3200$ | $t = 3400$ | $t = 3600$ | $t = 3800$ | $t = 4000$ |

Figure 10: The solution from fig.8 at larger time: during the second transient regime (top row) the clusters appear in shifting patterns that lose symmetry and gradually become more irregular; in the third transient regime (bottom row) the horizontal bands smooth out and slowly adjust their spacing. This yields a quasi 1–dimensional SW for $t > 4000$.
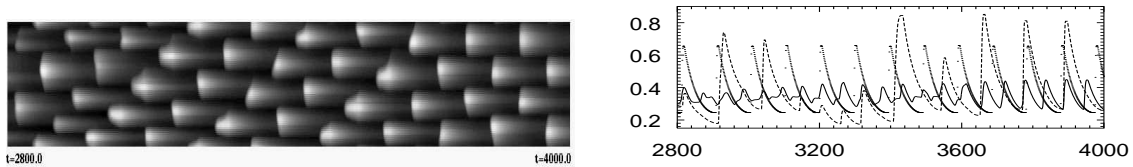

Figure 11: Diagnostics for fig.10. Left: diagonal line data; right: time–series, $\langle \theta_{1 \times 1} \rangle(t)$, $\theta_{1 \times 1}(t, \vec{x}_1)$ (dashed), $\theta_{1 \times 1}^{\mathrm{ODE}}(t)$ (short dashes); $\vec{x}_1$ is the same point as marked in fig.3.

3.4 Random initial conditions

In 1D, random initial data yields, depending on the parameters, regular periodic PC, SW or PW, similar to the solutions in fig.2: after a rather short transient the solutions become periodic. Since, as illustrated in section 3.3, in 2D transients may be very long, it is worthwhile to study how random initial data evolve in 2D. Therefore, we set

$$X_l|_{t=0}(i, j) = r_{i,j,l} \, z_l \qquad (3.1)$$

where each $r_{i,j,l}$ is a (pseudo)random number between 0.5 and 1.5. Choosing a new $r_{i,j,l}$ for each (i, j) tends to yield the synchronized solution X_{BO}. Hence the initial data was *preclustered* by choosing the same $r_{i,j,l}$ on squares of certain side lengths q.
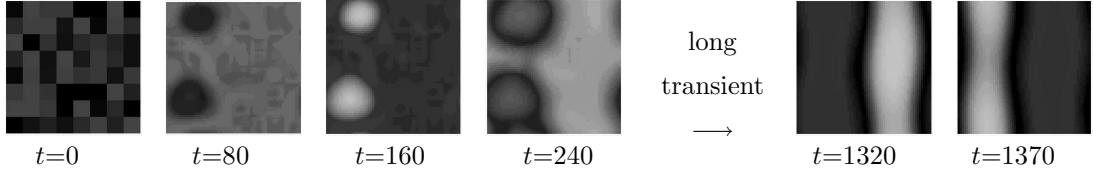
12

Figure 12: $\vec{E} = (28, 24, 15, 18)$, random initial data according to (3.1) with $q = 8$; greyscale snapshots of $\theta_{1 \times 1}$, $z_{\mathrm{scal}} = 0.2, 1$. Initial evolution and large time 1-dimensional PC; the vertical clusters smoothen out for still larger t and yield a perfectly periodic solution.

In the parameter regime of table 1, this yields, after a sufficiently long transient, quasi-1D PC solutions with either horizontal or vertical clusters. Again it was checked that these are really PC and not SW by running the simulations on larger domains and with different values q for the preclustering. An example with $q = 8$ is shown in fig.12.

More interesting solution are obtained in the standing wave regime $\vec{E} = (30, 22, 15, 18)$ on large domains. In fig.13 we set $n = 128$ and $q = 8$. The top row shows how initially the random initial data is locally smoothed out. Then rather irregular clusters appear on a spatial scale of again approximately 0.005cm. This is further illustrated in the bottom row and in the diagnostics in fig.14. This clustering continues in an irregular way (no qualitative change was observed up to simulation time $t = 4000$). Moreover, the individual clusters can only roughly be grouped into two common phases. In the time series this results in a very smeared out and irregular $\langle \theta_{1 \times 1} \rangle$ which only roughly "oscillates" with twice the ODE period and with a rather small amplitude. It appears reasonable to call this regime *standing wave turbulence* since on smaller domains the parameters yield standing wave solutions as illustrated in sec.3.3. However, correlation and further statistical analysis for these solutions remains to be done.
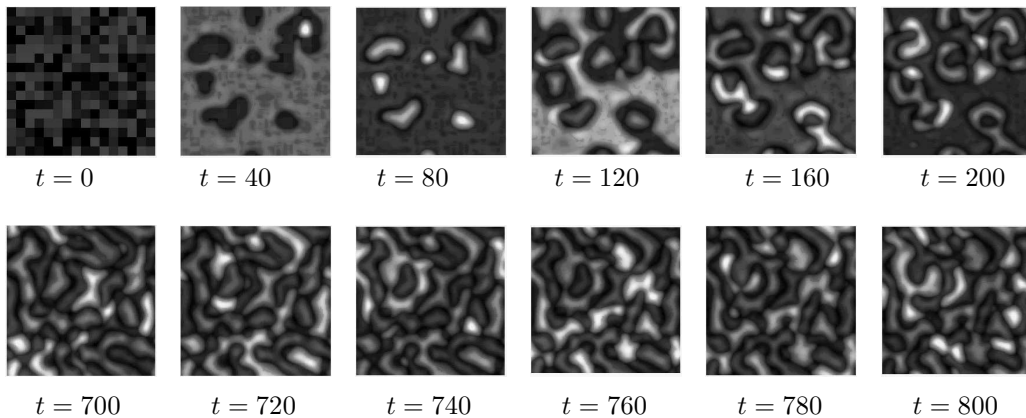

Figure 13: $n = 128, \delta = 0.0005$cm, $\vec{E} = (30, 22, 15, 18)$, random initial data according to (3.1) with $q = 8$; greyscale snapshots of $\theta_{1 \times 1}$, $z_{\mathrm{scal}} = 0.2, 1$. Initial evolution (top row) and irregular small scale clustering at larger time (bottom row); see also fig.14.
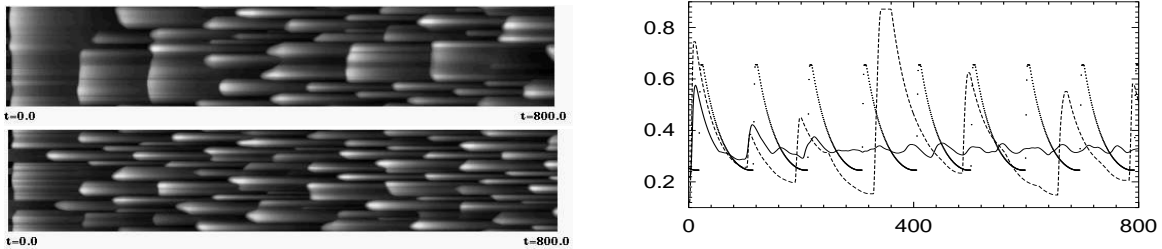
Figure 14: Diagnostics for fig.13: vertical (top left) and diagonal (bottom left) line data, $\langle \theta_{1\times1} \rangle$, $\theta_{1\times1}(\vec{x}_1)$ (dashed), $\theta_{1\times1}^{\mathrm{ODE}}$ (points), with $\vec{x}_1 = (8\delta, 8\delta)$ as in fig.3.

4 Conclusions

We have presented examples for 4 different types of behavior of solutions of (1.2). In a number of further simulations we confirmed for the 2D case studied here the conclusions about the parameter dependence of (1.2) studied in 1D in [23]. Briefly, these can be summarized as follows:

(a) For the diffusion energies in table 1 we obtain PC solutions, provided the initial perturbations of a homogenous surface near the periodic ODE orbit are large enough.

(b) Decreasing diffusion of $\theta_{\mathrm{NO}}^{1\times1}$ and/or increasing diffusion of $\theta_{\mathrm{NO}}^{\mathrm{hex}}$ first introduces and then decreases a spatial length scale for the clusters, i.e., it shifts the system to the SW regime.

(c) One key ingredient of both PC and SW is the relatively fast diffusion of $\theta_{\mathrm{NH_3}}^{1\times1}$ and $\theta_{\mathrm{H}}^{1\times1}$. For slower diffusion of $\theta_{\mathrm{NH_3}}^{1\times1}, \theta_{\mathrm{H}}^{1\times1}$ no clustering appears but phase waves. This is in contrast to $CO+O_2$ on Pt(110) [1, 7, 8, 19, 18, 3, 5, 4], where clustering has only been reported under a global coupling through the gas phase. This global coupling is replaced here by the fast diffusion of $\theta_{\mathrm{NH_3}}^{1\times1}, \theta_{\mathrm{H}}^{1\times1}$.

(d) Temperature dependence: at lower temperatures, synchronization and PW dominate over PC and SW. Conversely, at higher temperatures clustering dominates over synchronization and PW. This shows that the second key ingredient for the clustering is the relaxation type of the ODE oscillations, which becomes sharper at larger T. However, the numerics also become more difficult at larger T and the system may fail due to violation of certain mass balances; see [23] for more details (in the 1D case).

The most important new feature in 2D are curvature effects. For generic initial data in the PC regime or the SW regime on small domains, the solution relaxes to quasi 1-dimensional PC or SW. This happens after a possibly very long transient during which the cluster boundaries slowly adjust. For small diffusion of $\theta_{\mathrm{NO}}^{1\times1}$ and/or high diffusion of $\theta_{\mathrm{NO}}^{\mathrm{hex}}$ on a large domain, a turbulent standing wave regime appears.

Here we gave phenomenological descriptions. Some ideas for the mathematical analysis of these patterns have been proposed in [23]. This will be subject of further research. It also remains to compare the 2D results reported here with experimental data [25]. To make this comparison more realistic a *global coupling* should possibly be included into the model.

A The ODE

To make the paper somewhat self contained, we give the ODE (1.1); see [14, 24] for the chemical meanings and discussion:

$$\frac{\mathrm{d}}{\mathrm{d}t}\theta_{\mathrm{NO}}^{1\times1} = \mathrm{F}_{\mathrm{NO}}\mathrm{p}_{\mathrm{NO}}(\theta_{1\times1} - \theta_{\mathrm{NO}}^{1\times1} - 4\theta_{\mathrm{NH_3}}^{1\times1}) - k_1\theta_{\mathrm{NO}}^{1\times1} - k_2\frac{\theta_{\mathrm{NO}}^{1\times1}\theta_{\mathrm{empty}}^{1\times1}}{\theta_{1\times1}} + k_3\theta_{\mathrm{NO}}^{\mathrm{hex}}\theta_{1\times1} , \tag{A.1a}$$

$$\frac{\mathrm{d}}{\mathrm{d}t}\theta_{\mathrm{NO}}^{\mathrm{hex}} = \mathrm{F}_{\mathrm{NO}}\mathrm{p}_{\mathrm{NO}}(\theta_{\mathrm{hex}} - \theta_{\mathrm{NO}}^{\mathrm{hex}}) - k_3\theta_{\mathrm{NO}}^{\mathrm{hex}}\theta_{1\times1} - k_4\theta_{\mathrm{NO}}^{\mathrm{hex}} , \tag{A.1b}$$

$$\frac{\mathrm{d}}{\mathrm{d}t}\theta_{1\times1} = \begin{cases} (\frac{\mathrm{d}}{\mathrm{d}t}\theta_{\mathrm{NO}}^{1\times1})/\theta_{\mathrm{grow}}^{1\times1} & \text{if } \frac{\mathrm{d}}{\mathrm{d}t}\theta_{\mathrm{NO}}^{1\times1} > 0 \text{ and } \theta_{\mathrm{NO}}^{1\times1} \geq \theta_{\mathrm{grow}}^{1\times1}\theta_{1\times1} \text{ and } \theta_{1\times1} < 1 , \\ -k_{11}(\theta_{1\times1} - \theta_{\mathrm{def}}^{\mathrm{hex}})(1-c) & \text{if } \theta_{1\times1} > \theta_{\mathrm{def}}^{\mathrm{hex}} \text{ and } \mathrm{c} < 1 , \\ 0 & \text{otherwise} , \end{cases} \tag{A.1c}$$

$$\frac{\mathrm{d}}{\mathrm{d}t}\theta_{\mathrm{NH_3}}^{1\times1} = \mathrm{F}_{\mathrm{NH_3}}\mathrm{p}_{\mathrm{NH_3}}(\theta_{1\times1} - 3\theta_{\mathrm{NH_3}}^{1\times1} - 1.6\theta_{\mathrm{NO}}^{1\times1}) - k_5\theta_{\mathrm{NH_3}}^{1\times1}$$
$$- k_6\frac{\theta_{\mathrm{NH_3}}^{1\times1}[\theta_{1\times1} - \theta_{\mathrm{H}}^{1\times1} - 2.5(\theta_{\mathrm{O}}^{1\times1} + \theta_{\mathrm{N}}^{1\times1})]}{\theta_{1\times1}} + k_7\frac{\theta_{\mathrm{N}}^{1\times1}\theta_{\mathrm{H}}^{1\times1}}{\theta_{1\times1}} , \tag{A.1d}$$

$$\frac{\mathrm{d}}{\mathrm{d}t}\theta_{\mathrm{O}}^{1\times1} = k_2\frac{\theta_{\mathrm{NO}}^{1\times1}\theta_{\mathrm{empty}}^{1\times1}}{\theta_{1\times1}} - k_8\frac{\theta_{\mathrm{O}}^{1\times1}\theta_{\mathrm{N}}^{1\times1}}{\theta_{1\times1}} , \tag{A.1e}$$

$$\frac{\mathrm{d}}{\mathrm{d}t}\theta_{\mathrm{N}}^{1\times1} = k_2\frac{\theta_{\mathrm{NO}}^{1\times1}\theta_{\mathrm{empty}}^{1\times1}}{\theta_{1\times1}} + k_6\frac{\theta_{\mathrm{NH_3}}^{1\times1}[\theta_{1\times1} - \theta_{\mathrm{H}}^{1\times1} - 2.5(\theta_{\mathrm{O}}^{1\times1} + \theta_{\mathrm{N}}^{1\times1})]}{\theta_{1\times1}} - k_7\frac{\theta_{\mathrm{N}}^{1\times1}\theta_{\mathrm{H}}^{1\times1}}{\theta_{1\times1}} - k_9\frac{(\theta_{\mathrm{N}}^{1\times1})^2}{\theta_{1\times1}} , \tag{A.1f}$$

$$\frac{\mathrm{d}}{\mathrm{d}t}\theta_{\mathrm{H}}^{1\times1} = \mathrm{F}_{\mathrm{H_2}}\mathrm{p}_{\mathrm{H_2}}\frac{[\theta_{1\times1} - \theta_{\mathrm{H}}^{1\times1} - 2.5(\theta_{\mathrm{O}}^{1\times1} + \theta_{\mathrm{N}}^{1\times1})]^2}{\theta_{1\times1}} + 3k_6\frac{\theta_{\mathrm{NH_3}}^{1\times1}[\theta_{1\times1} - \theta_{\mathrm{H}}^{1\times1} - 2.5(\theta_{\mathrm{O}}^{1\times1} + \theta_{\mathrm{N}}^{1\times1})]}{\theta_{1\times1}}$$
$$- 3k_7\frac{\theta_{\mathrm{N}}^{1\times1}\theta_{\mathrm{H}}^{1\times1}}{\theta_{1\times1}} - 2k_8\frac{\theta_{\mathrm{O}}^{1\times1}\theta_{\mathrm{H}}^{1\times1}}{\theta_{1\times1}} - k_{10}\frac{(\theta_{\mathrm{H}}^{1\times1})^2}{\theta_{1\times1}} . \tag{A.1g}$$

The three conditions on the right hand side of (A.1c) have to be read top down and the first one fulfilled determines the right hand side. The rate constants $k_1, \ldots, k_{11}$ are determined by Arrhenius–law $k_i = \nu_i \mathrm{e}^{-E_i/RT}$, where the ν_i and most of the E_i are constants, given in table 2. For E_1 and E_5 coverage–dependent nonlinear corrections are used in the form

$$E_1 = E_1^0 - 24(\theta_{\mathrm{NO}}^{1\times1}/\theta_{1\times1})^2, \quad E_5 = E_5^0 - 30(\theta_{\mathrm{NH_3}}^{1\times1}/\theta_{1\times1})^2. \tag{A.2}$$

The auxiliary functions in (A.1) are given by

$$\theta_{\text{empty}}^{1\times1} = \max\left[(\theta_{1\times1} - \frac{\theta_{\text{NO}}^{1\times1}}{\theta_{\text{NO}}^{\text{inh}}} - \frac{\theta_{\text{O}}^{1\times1}}{\theta_{\text{O}}^{\text{inh}}}), 0\right] + \max[(\theta_{\text{def}}^{1\times1} - \theta_{\text{O}}^{1\times1}), 0],$$

$$c = \left(\frac{\theta_{\text{NO}}^{1\times1}}{\theta_{\text{NO}}^{\text{crit}}} + \frac{\theta_{\text{O}}^{1\times1}}{\theta_{\text{O}}^{\text{crit}}}\right)/\theta_{1\times1}, \quad \theta_{1\times1} + \theta_{\text{hex}} = 1, \quad \theta_{\text{def}}^{1\times1} = \theta_{1\times1}\theta_{\text{def}}, \quad \theta_{\text{def}}^{\text{hex}} = \theta_{\text{hex}}\theta_{\text{def}},$$

and the further parameters are given in table 3.

reaction step	param.	ν_i (s^{-1})	E$_i$ (kcal $\times$ mol^{-1})	value at 420K (s^{-1})
NO–desorption 1x1	k_1	1.7×10^{14}	37.0^a	9.7×10^{-6}
NO–dissociation 1x1	k_2	2.0×10^{15}	28.5	3.0
NO–trapping on 1x1	k_3	2.2×10^{4}	8.0	1.52
NO–desorption hex	k_4	4.0×10^{12}	26.0	0.12
NH$_3$–desorption 1x1	k_5	1.0×10^{9}	18.0^a	0.43
NH$_3$–dissociation 1x1	k_6	1.0×10^{15}	27.5	4.98
NH$_3$–formation 1x1	k_7	1.0×10^{10}	16.0	47.7
H$_2$O–formation 1x1	k_8	1.0×10^{13}	13.0	1.73×10^6
N$_2$–desorption 1x1	k_9	1.3×10^{12}	19.0	1.70×10^2
H$_2$–desorption 1x1	k_{10}	8.0×10^{12}	23.0	8.72
Transition 1x1$\rightarrow$hex	k_{11}	2.5×10^{11}	25.0	2.48×10^{-2}

^{a} for zero local coverage, see (A.2).

Table 2: Rate constants for the NO+NH3 reactions on Pt(100).

description	param.	value
NO–adsorption flux 1×1, hex	F_{NO}	2.21×10^5(mbar^{-1}s^{-1})
NH$_3$–adsorption flux 1×1	F_{NH_3}	2.84×10^5(mbar^{-1}s^{-1})
H$_2$–adsorption flux 1×1	F_{H_2}	8.28×10^5(mbar^{-1}s^{-1})
Inhibition coverage of NO for NO–dissociation	$\theta_{\text{NO}}^{\text{inh}}$	0.61
Inhibition coverage of O for NO–dissociation	$\theta_{\text{O}}^{\text{inh}}$	0.399
Critical coverage of NO for the $1\times1\rightarrow$ hex phase transf.	$\theta_{\text{NO}}^{\text{crit}}$	0.3
Critical coverage of NO for the $1\times1\rightarrow$ hex phase transf.	$\theta_{\text{O}}^{\text{crit}}$	0.4
Coverage for island growth in the hex$\rightarrow 1\times1$ phase transf.	$\theta_{\text{grow}}^{1\times1}$	0.5
Amount of surface defects	θ_{def}	1.0×10^{-4}
partial pressures (tunable, but kept fixed here)	p_{NO}	1.1×10^{-6} mbar
	p_{NH_3}	4.7×10^{-6} mbar

Table 3: Temperature independent parameters.

References

[1] M. Bär, M. Hildebrand, M. Eiswirth, M. Falcke, H. Engel, and M. Neufeld. Chemical turbulence and standing waves in a surface reaction model: The influence of global coupling and wave instabilities. *Chaos*, 4:499–508, 1994.

[2] J.V. Barth. Transport of adsorbates at metal surfaces : From thermal migration to hot precursors. *Surf. Sci. Rep.*, 40(3–5):75–149, 2000.

[3] M. Bertram and A. S. Mikhailov. Pattern formation in a surface chemical reaction with global delayed feedback. *Phys. Rev. E*, 63:066102, 2001.

[4] M. Bertram and A. S. Mikhailov. Pattern formation on the edge of chaos: Experiments with CO oxidation on a Pt(110) surface under global delayed feedback. *Phys. Rev. E*, 67:036208, 2003.

[5] M. Bertram and A. S. Mikhailov. Pattern formation on the edge of chaos: Mathematical modeling of CO oxidation on a Pt(110) surface under global delayed feedback. *Phys. Rev. E*, 67:036207, 2003.

[6] P. Deuflhard and F. Bornemann. *Scientific computing with ordinary differential equations*, volume 42 of *Texts in Applied Mathematics*. Springer-Verlag, New York, 2002.

[7] M. Falcke and H. Engel. Pattern formation during the CO oxidation on Pt(110) surfaces under global coupling. *J. Chem. Phys.*, 101:6255–6263, 1994.

[8] M. Falcke, H. Engel, and M. Neufeld. Cluster formation, standing waves, and stripe patterns in oscillatory active media with local and global coupling. *Phys. Rev. E*, 52:763–771, 1995.

[9] E. M. Izhikevich. Phase equations for relaxation oscillators. *SIAM J. Appl. Math.*, 60(5):1789–1804, 2000.

[10] M. Kim, M. Bertram, M. Pollmann, A. von Oertzen, A. Mikhailov, H. H. Rotermund, and G. Ertl. Controlling chemical turbulence by global delayed feedback: Pattern formation in catalytic CO oxidation reaction on Pt(110). *Science*, 292:1357–1359, 2001.

[11] S. Krömker. Wave bifurcation in models for heterogeneous catalysis. *Acta Math. Univ. Comenian. (N.S.)*, 67(1):83–100, 1998.

[12] Y. Kuramoto. *Chemical oscillations, waves, and turbulence*, volume 19 of *Springer Series in Synergetics*. Springer-Verlag, Berlin, 1984.

[13] Y. Kuramoto, H. Nakao, and D. Battogtokh. Multi-scaled turbulence in large populations of oscillators in a diffusive medium. *Phys. A*, 288(1-4):244–264, 2000.

[14] S.J. Lombardo, T. Fink, and R. Imbihl. Simulations of the $NO+NH_3$ and $NO+H_2$ reactions on Pt(100): Steady state and oscillatory kinetics. *J. Chem. Phys*, 98(7):5526–5539, 1993.

[15] A. S. Mikhailov. *Foundations of synergetics I. Distributed active systems*. Springer-Verlag, Berlin, 1990.

[16] V. I. Nekorkin and M. G. Velarde. *Synergetic phenomena in active lattices – Patterns, waves, solitons, chaos*. Springer-Verlag, Berlin, 2002.

[17] E. M. Nicola, M. Or-Guil, W. Wolf, and M. Bär. Drifting pattern domains in a reaction-diffusion system with nonlocal coupling. *Phys. Rev. E*, 65:055101(R), 2002.

[18] A. v. Oertzen, H. H. Rotermund, A. S. Mikhailov, and G. Ertl. Standing wave patterns in the CO oxidation reaction on a Pt(110) surface: Experiments and modeling. *J. Phys. Chem. B*, 104(14):3155–3178, 2000.

[19] K.C. Rose, D. Battogtokh, A. Mikhailov, R. Imbihl, W. Engel, and A.M. Bradshaw. Cellular structures in catalytic reactions with global coupling. *Phys. Rev. Lett.*, 76:3582–3585, 1996.

[20] E.G. Seebauer and C.E. Allen. Estimating surface diffusion coefficients. *Progress in Surface Science*, 49:265–330, 1995.

[21] D. Somers and N. Kopell. Waves and synchrony in networks of oscillators of relaxation and non-relaxation type. *Phys. D*, 89(1-2):169–183, 1995.

[22] H. Uecker. Movies for NO+NH$_3$ on Pt(100), `www.math.uni-karlsruhe.de/~uecker/chem/`. 2003.

[23] H. Uecker. Standing waves, clustering, and phase waves in 1D simulations of kinetic relaxation oscillations in NO+NH$_3$ on Pt(100). Accepted by *Physica D*, 2003.

[24] H. Uecker, R. Imbihl, M. Rafti, I.M. Iruzun, J. L. Vicente, and E.E. Mola. Adiabatic reduction and hysteresis of the LFI–model of NO+NH$_3$ on Pt(100). *Chem. Phys. Let.*, 382:232–244, 2003.

[25] G. Veser, F. Esch, and R. Imbihl. Regular and irregular spatial patterns in the catalytic reduction of NO with NH$_3$ on Pt(100). *Catalysis Letters*, 13:371–382, 1992.

[26] D. Walgraef. *Spatio–Temporal Pattern Formation*. Springer Verlag New York, 1997.

[27] L. Yang, M. Dolnik, A. M. Zhabotinsky, and I. R. Epstein. Oscillatory clusters in a model of the photosensitive Belousov-Zhabotinsky reaction system with global feedback. *Phys. Rev. E*, 62:6414–6420, 2000.

[28] A. M. Zhabotinsky, M. Dolnik, and I. R. Epstein. Pattern formation arising from wave instability in a simple reaction-diffusion system. *J. Chem. Phys.*, 103(23):10306–10314, 1995.